Chetty *et al. Alzheimer's Research & Therapy* (2024) 16:236
https://doi.org/10.1186/s13195-024-01582-w

Alzheimer's Research & Therapy

RESEARCH Open Access

EEG biomarkers in Alzheimer's and prodromal Alzheimer's: a comprehensive analysis of spectral and connectivity features

Chowtapalle Anuraag Chetty[1†], Harsha Bhardwaj[1,8†], G. Pradeep Kumar[1†], T. Devanand[1], C. S. Aswin Sekhar[1], Tuba Aktürk[2], Ilayda Kiyi[3], Görsev Yener[4,5,6], Bahar Güntekin[2,7], Justin Joseph[1] and Chinnakkaruppan Adaikkan[1*]

Abstract

Background Biomarkers of Alzheimer's disease (AD) and mild cognitive impairment (MCI, or prodromal AD) are highly significant for early diagnosis, clinical trials and treatment outcome evaluations. Electroencephalography (EEG), being noninvasive and easily accessible, has recently been the center of focus. However, a comprehensive understanding of EEG in dementia is still needed. A primary objective of this study is to investigate which of the many EEG characteristics could effectively differentiate between individuals with AD or prodromal AD and healthy individuals.

Methods We collected resting state EEG data from individuals with AD, prodromal AD, and normal cognition. Two distinct preprocessing pipelines were employed to study the reliability of the extracted measures across different datasets. We extracted 41 different EEG features. We have also developed a stand-alone software application package, *Feature Analyzer*, as a comprehensive toolbox for EEG analysis. This tool allows users to extract 41 EEG features spanning various domains, including complexity measures, wavelet features, spectral power ratios, and entropy measures. We performed statistical tests to investigate the differences in AD or prodromal AD from age-matched cognitively normal individuals based on the extracted EEG features, power spectral density (PSD), and EEG functional connectivity.

Results Spectral power ratio measures such as theta/alpha and theta/beta power ratios showed significant differences between cognitively normal and AD individuals. Theta power was higher in AD, suggesting a slowing of oscillations in AD; however, the functional connectivity of the theta band was decreased in AD individuals. In contrast, we observed increased gamma/alpha power ratio, gamma power, and gamma functional connectivity in prodromal AD. Entropy and complexity measures after correcting for multiple electrode comparisons did not show differences in AD or prodromal AD groups. We thus catalogued AD and prodromal AD-specific EEG features.

†Chowtapalle Anuraag Chetty, Harsha Bhardwaj and Pradeep Kumar G contributed equally to this work.

*Correspondence:
Chinnakkaruppan Adaikkan
chinna@cbr-iisc.ac.in

Full list of author information is available at the end of the article

Conclusions Our findings reveal that the changes in power and connectivity in certain frequency bands of EEG differ in prodromal AD and AD. The spectral power, power ratios, and the functional connectivity of theta and gamma could be biomarkers for diagnosis of AD and prodromal AD, measure the treatment outcome, and possibly a target for brain stimulation.

Keywords EEG-based biomarker, Theta-alpha power ratio, Gamma, Eyes closed EEG, Slowing of oscillations, Pairwise phase consistency, Brain connectivity, Aging

Background

Alzheimer's disease (AD) is a progressive neurodegenerative disease, and its prevalence is rapidly increasing worldwide. The progression of AD has three phases: it starts with the preclinical asymptomatic stage, develops into mild cognitive impairment (MCI) due to AD, and finally, Alzheimer's dementia. Currently, there is no cure for AD, and it creates an enormous socioeconomic burden worldwide [1]. Therefore, early diagnosis and effective treatment of AD have been investigated at multiple levels.

Aberrant accumulation of amyloid plaques due to amyloidβ (Aβ) peptide [2] and neurofibrillary tangles by hyper-phosphorylated tau [3], microglia- and astrocyte-mediated inflammation [4], compromised blood-brain barrier [5] and the loss of neurons and synapse [6] are shown to develop with disease progression. Specifically, amyloid and tau accumulation starts in the preclinical stages and MCI [7–9], while neurodegeneration occurs later in the disease progression and is robustly associated with memory impairments [10]. Blood-based markers, including Aβ40, Aβ42, and phosphorylated tau, have now been explored as biomarkers for MCI and AD [11]. Because changes in electroencephalography (EEG) activity during memory processes have been well documented [12], MCI and AD-specific EEG biomarkers have received greater attention recently.

EEG is noninvasive and inexpensive; therefore, it has been suggested that the financial burden of implementing widespread screening based on EEG biomarkers will be relatively low if such biomarkers are available [13]. Several recent studies examining specific features in EEG showed evidence for reduced EEG complexity [14] (e.g., Lyapunov Exponent [15], Hjorth complexity [16]), changes in entropy measures (e.g., Permutation entropy [17], Sample entropy [18]), slowing of oscillations (e.g., delta/alpha ratio [19], spectral power ratio [20]) and changes in connectivity (e.g., coherence [21]) in AD. While these observations are interesting, most studies have examined only a specific group of features and their significance. Comprehensive evaluations that have covered all possible EEG features are limited. Such a comprehensive analysis will facilitate choosing the best feature suitable for preclinical and clinical settings [22]. Also, recent guidelines suggest the need for monitoring changes in biomarkers while assessing the efficacy of candidate drugs and interventions [23]. Tools for the objective analysis of EEG would facilitate evaluating and finding noninvasive biomarkers for AD or prodromal AD. Such biomarkers would also allow for determining the efficacy of candidate drugs or neurostimulation.

Most of the automated methods employed to distinguish AD use many possible features as input to the machine learning (ML) classifiers without the significance check. In such models, the feature vector may contain insignificant features as well. Including insignificant features increases the size of the input and subsequent layers of neural network classifiers, causing computational overhead and thereby degrading the performance. Knowledge regarding the features that are determinant enough to distinguish AD from healthy controls helps to simplify the architecture of artificial neural network (ANN) models and reduce training/testing time, as determinant features can be selectively used to drive the models. In addition, the factors that drive the clinical decision need to be known or established as per the mandates of evidence-based medicine. However, rather than ML models employed for the diagnosis of AD that use many possible EEG features as input, comprehensive studies that explore the discriminant ability of the features to identify the potential EEG biomarkers are rare. Therefore, we explored the discriminant ability of EEG features from all possible categories namely, descriptive statistics, impulsive metrics, spectral descriptors, spectro-temporal features, signal complexity measures, and brain connectivity metrics. In addition, we have analyzed the influence of two such preprocessing pipelines on the discriminant ability of EEG features.

Here, we comprehensively investigated the differences in EEG characteristics in AD or prodromal AD compared to cognitively normal individuals across several datasets. Although amyloid and tau tangles accumulate more as MCI and AD progress, our results suggest that oscillatory activity and functional connectivity differences occur uniquely in prodromal AD and AD.

Methods

Study subjects and data collection

The present study used resting-state EEG data from 3 independent datasets: Cohort 1 comprises 46 healthy control and 46 AD subjects [24], Cohort 2 comprises 29 control and 36 AD subjects [25], and Cohort 3

comprises 30 control and 30 prodromal AD subjects [17]. The Cohort 2 dataset is publicly available, whereas we recently generated Cohort 1 and 3 datasets [17, 24]. In addition to AD or MCI due to AD (i.e., prodromal AD) diagnosis, mini-mental state examination (MMSE) from all subjects was also available. The Supplementary Methods describes the detailed subject inclusion, exclusion criteria, and information regarding the data acquisition. The resting-state EEG data was collected in accordance with the international 10–20 electrode placement system. The sampling frequency of all three cohorts was 500 Hz.

EEG data preprocessing

Preprocessing EEG data to remove artifacts in the signal, such as bad electrodes/channels and segments, is vital for obtaining reliable results [13]. The impact of noise and artifacts on the outcome of the objective analysis of EEG, and the need for preprocessing are demonstrated by Robbins et al. [26] and Coelli et al. [27]. A variety of preprocessing pipelines [28] have emerged to alleviate the negative impacts caused by the artifacts. Among the pipelines, the ability of the Artifact Subspace Reconstruction (ASR) to improve the quality of EEG and its performance over other candidate preprocessing pipelines is reported in the literature [29]. However, the ASR has some limitations including setting the threshold values for different parameters and residues of the suppressed transients left over in the pre-processed signal. Baseline wandering (motion artifacts) and transients (spikes) are two major artifacts seen in EEG. The potential of the local detrending in removing the baseline wandering [30] and the Hampel filter in suppressing the outlier spikes in EEG [31] are already appreciated in the literature. However, the impact of the combination of local detrending and the Hampel filter (det-Hamp in the present study) on the outcome of the objective analysis of EEG and its performance in comparison with the ASR has not been studied yet. Therefore, we pre-processed EEG data using two different pipelines to improve the quality of EEG and for better interpretations. Specifically, we used (1) the det-Hamp pipeline (detrending followed by Hampel filtering) [33] in MATLAB with Chronux 2.0 toolbox [34] and custom MATLAB codes (see supplementary Methods) and (2) artifact subspace reconstruction (ASR) in MATLAB using the EEGLAB plug-in function [32]. The ASR pipeline is widely used in the field [35] to suppress the artifacts and remove the distortions in the EEG data. EEG data was filtered in the range spanning 0.5–48 Hz using a bandpass filter for both the ASR and det-Hamp pipeline before further analysis. One-minute resting-state eyes-closed EEG data was used for all further analysis. Specifically, the first 10 s immediately after the eyes closed was not included in the analysis, but the following one minute was chosen consistently across all subjects and cohorts. EEG was analyzed in different canonical frequency bands: delta (1–4 Hz), theta (5–8 Hz), alpha (9–13 Hz), beta (14–30 Hz), and gamma (31–48 Hz).

EEG feature analysis

We evaluated 41 distinct EEG features. These features belong to various groups, including temporal attributes, spectral descriptors, complexity measures, wavelet-based features, power ratios, and entropy measures. Temporal domain [36, 37] features include Variance, Skewness, Kurtosis, Shape Factor, Peak Amplitude, Impulse Factor, Crest Factor, Clearance Factor, Willison's Amplitude, and Zero-crossing Rate. Entropy measures [38, 39] include Sample Entropy, Approximate Entropy, Permutation Entropy, and State Space Correlation Entropy. Complexity measures [40] include the Correlation Dimension, Higuchi Fractal Dimension, Katz Fractal Dimension, Lyapunov Exponent, Hurst Exponent, Lempel-Ziv Complexity, Hjorth Activity, Hjorth Mobility, and Hjorth Complexity. Spectral Descriptors [37, 41] include Alpha Dominant Frequency, Gamma Dominant Frequency, Spectral Roll-off, Spectral Centroid, Spectral Spread, Spectral Flux, Spectral Skewness, and Spectral Kurtosis. Power Ratios [20, 42, 43] include the Theta Beta, Theta Alpha, Gamma Alpha and Spectral Power ratios. Wavelet Energy features [44] include Approximate Wavelet Energy, Detailed Wavelet Energy, Relative Wavelet Energy, Approximate Wavelet Packet Energy, Detailed Wavelet Packet Energy, and Relative Wavelet Packet Energy. Custom MATLAB codes (see the Resource section) were used to extract all these features. These features are explained in detail in the Supplementary Methods section.

Power spectral density (PSD) and pairwise phase consistency (PPC)

PSD was estimated using a multi-taper method with a single Slepian taper using the 'mtspectrum' function of the Chronux toolbox [34]. Absolute power was used for further analysis. PPC analysis was conducted across frequencies ranging from 1 to 48 Hz with a resolution of 1 Hz using custom MATLAB codes and the Fieldtrip Toolbox [45] following a method described previously [46].

Statistics

All analyses were performed using MATLAB or Prism (GraphPad version 9.3). As detailed below, different statistical tests were employed based on the data distribution. An unpaired two-tailed t-test was used to investigate the statistical differences in age, MMSE, and years of education between the two groups. ANOVA with Tukey's multiple comparison correction was used to test MMSE differences between groups and sex. The Wilcoxon

Rank-sum test [47, 48] equivalent to the Mann-Whitney U test was performed in MATLAB to examine the statistical differences of EEG features, PSD, and PPC between control and disease states. False discovery rate (FDR) correction was done using the Benjamin and Hochberg method [49]. FDR correction was done across electrodes for EEG features and PPC, and across frequency bins for PSD. Spearman's rank correlation [50] was computed in MATLAB to examine the degree of correlation between EEG features and MMSE scores at all electrodes. A significance level of $P<0.05$ was set for all statistical tests.

Results

Categories of EEG features

To examine which of the many EEG features could robustly distinguish AD from healthy subjects that could be explored as biomarkers (Fig. 1), we have written MATLAB algorithms and verified them on simulated time series signals (Supplementary Fig. 1A-1 C). We used age-matched healthy control (69.26±0.96; $N=46$) and AD subjects (70.96±0.81; $N=46$) of Cohort 1 (Supplementary Fig. 2A). The years of education did not differ between control (9.739±0.77) and AD subjects (8.106±0.71) (Supplementary Fig. 2B). As expected MMSE was significantly lower in AD (20.30±0.53) compared to healthy subjects (28.50±0.24) (Supplementary Fig. 2C). Lower MMSE were observed in both male and female AD subjects compared to the healthy subjects (Supplementary Fig. 2D).

Slowing of neural oscillations in AD

We extracted the EEG features from Cohort 1 and tested significant differences using the Rank-sum test ($P<0.05$ with FDR correction). We observed that the power ratios showed robust differences compared to the other features (Fig. 2A). Theta/alpha (4–8 Hz/ 9–13 Hz) and theta/beta (power of 4–8 Hz/ 14–30 Hz) ratios significantly distinguish AD from controls across many scalp locations (Fig. 2A). We next investigated the directionality of the power ratio difference between the controls and AD subjects. Topographic distributions of power ratios shown in Fig. 2B reveal that the theta/alpha and theta/beta ratios were higher in AD compared to age-matched healthy subjects (Fig. 2B and C) in both ASR and det-Hamp pipeline, suggesting a power increase in 4–8 Hz compared to alpha or beta in AD.

We next used the SHAP to cross-validate the Rank-sum test results because when multiple features are used as input to ANN classifiers via SHAP analysis, the relative importance of individual features and their role in decision-making can be understood. The ANN trained with the 41 features offered classification accuracies of 72.66% and 79.19%, respectively, for the det-Hamp and ASR pipelines. From SHAP, we observed that the power ratio category contributed the most to the classification (Fig. 2D). Theta/alpha, theta/beta, and spectral power ratios were found to be majorly contributing to the decision-making commonly in both preprocessing pipelines (Supplementary Fig. 3). These observations demonstrate an overall increase in the power of lower frequencies compared to higher frequencies in AD, consistent with

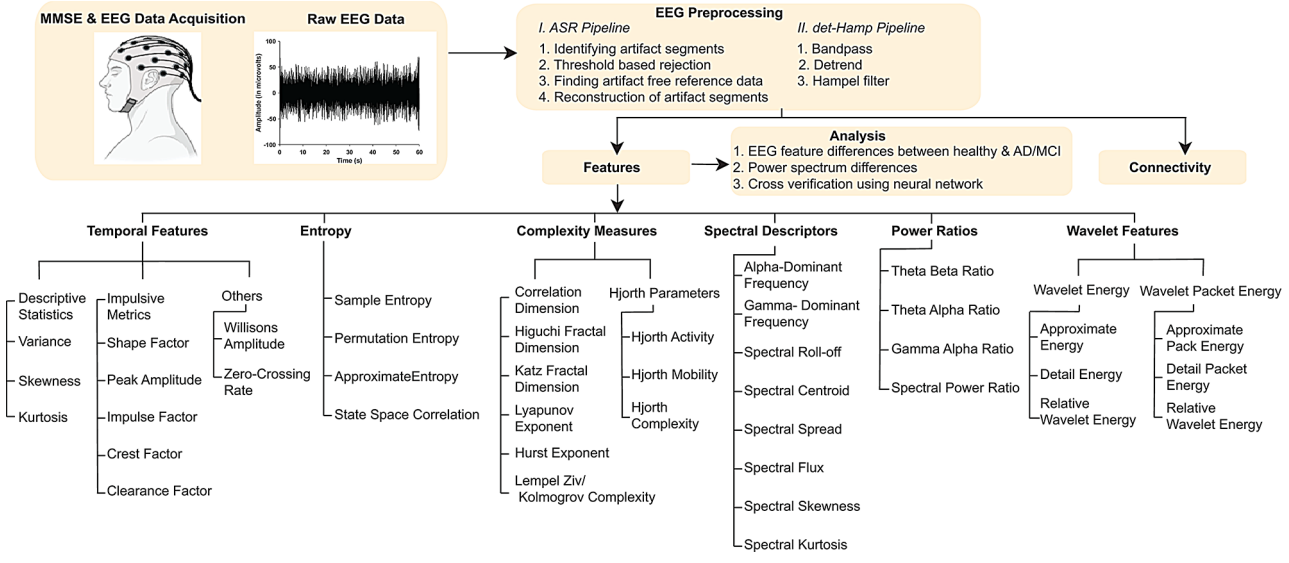

Fig. 1 Studying the relationship between EEG and cognition. The schematic shows the outline of the data pre-processing, EEG feature extraction, and analysis. At the bottom, a comprehensive cataloging and classification of various EEG features extracted and analyzed are shown (see Supplementary Methods)

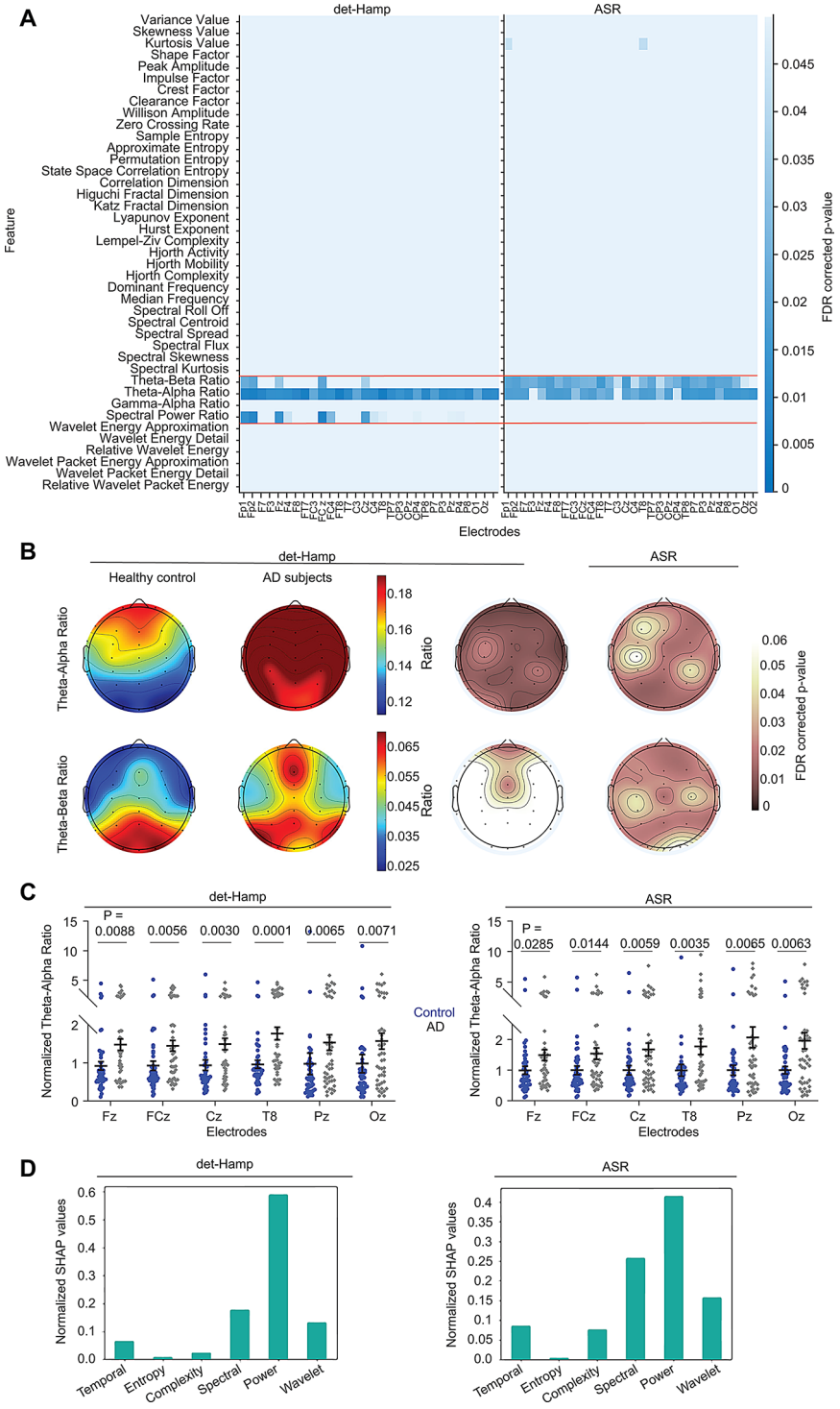

Fig. 2 Widespread power ratio changes in AD. (**A**) Heatmaps show Wilcoxon Rank-sum test differences of EEG features between control and AD for the det-Hamp (left) and ASR (right) pipelines after FDR correction. Scalp electrodes (channels) and EEG features are shown on the horizontal (X) and vertical (Y) axes, respectively. Power ratios that show robust differences are highlighted (orange line). (**B**) Topographical plots show the distribution of the theta/alpha power ratio (top) and theta/beta power ratio (bottom), averaged across all subjects in healthy control (left) and AD (middle left). Statistically significant scalp locations sustaining FDR correction are shown for the det-Hamp (middle right) and ASR (right) pipelines. (**C**) The normalized theta/alpha ratio for representative electrodes for the det-Hamp (left) and ASR pipelines (right, Wilcoxon Rank-sum test). Data points represent subjects. (**D**) The normalized cumulative mean of absolute SHAP values for det-Hamp and ASR pipelines are shown

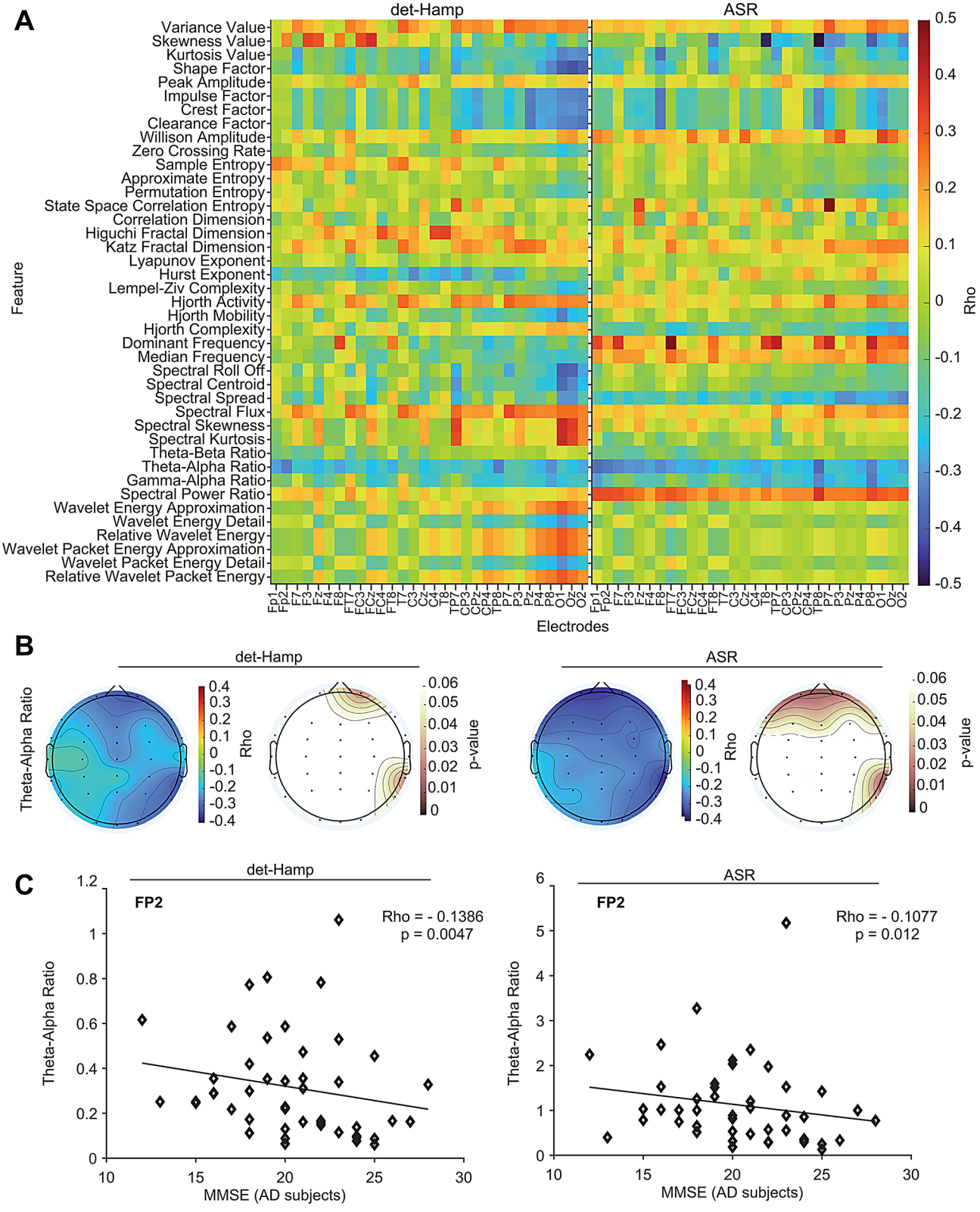

Fig. 3 Correlation of EEG features with MMSE scores in AD subjects. (**A**) Heatmaps show Spearman's rank correlation between EEG features and MMSE of AD subjects using det-Hamp (left) and ASR (right) pipelines. (**B**) Topographical plots show the correlation between theta/alpha power ratio and MMSE across all electrodes using det-Hamp (left) and ASR (middle right) pipelines. Correlations with significant P values using det-Hamp (left middle) and ASR (right) are shown. (**C**) The correlation between theta/alpha power ratio and MMSE of AD subjects for representative FP2 electrode (rho = -0.1386, $P = 0.0047$) or ASR (rho = -0.1077, $P = 0.012$) pipelines are shown

the hypothesis of slowing neural oscillations in AD [51, 52].

To assess the dependency between the EEG features and the MMSE scores, we computed Spearman's correlation coefficient (Fig. 3A). We used all 46 AD subjects of Cohort 1 and observed that EEG power ratios were markedly correlated with MMSE (Fig. 3A and B), consistent with the Rank-sum test results. Specifically, the theta/alpha ratio was negatively correlated with MMSE scores across many brain areas in AD subjects (Fig. 3A and C), suggesting that increased power in the theta frequency negatively correlates with MMSE in AD subjects.

To investigate whether these results can be replicated, we used another independent Cohort 2 dataset [25] (Supplementary Fig. 4A, 4B). The results in Cohort 2 also revealed a widespread increase in theta/alpha and theta/beta ratios across frontal, central, temporal, parietal, and occipital areas in AD (Supplementary Fig. 4C). Negative correlation between theta/alpha ratio and MMSE was also evident in AD subjects of Cohort 2 (Supplementary Fig. 4D, 4E). Thus, results in both cohorts point to slowing oscillations (more power in lower frequency bands) in AD.

Increased slow-gamma oscillations in prodromal AD

To test whether prodromal AD subjects also show differences in EEG features, we used age-matched 30 healthy and 30 MCI (prodromal AD) subjects of Cohort 3 (Supplementary Fig. 5). We observed significantly higher gamma/alpha ratio in left-frontal, frontocentral, central, and parietal brain areas in prodromal AD (Fig. 4A, B and C). Increased gamma/alpha ratio in prodromal AD individuals was consistent across both the preprocessing pipelines (Fig. 4A). We should note that gamma/alpha ratio did not show any difference in AD (Fig. 2A). Further, to cross-validate the power ratio differences in prodromal AD, we performed ANN analysis. We observed 74.88% (det-Hamp) and 83.99% (ASR) classification accuracies with SHAP analysis revealing power ratios contribute predominantly to the model (Fig. 4D). Taken together, these findings suggest that power ratios carry sufficient information to distinguish prodromal AD from healthy subjects.

Increased theta power in AD and gamma power in prodromal AD

To examine whether the increased power in theta compared to alpha in AD and increased gamma power relative to alpha in prodromal AD suggest any total power change in these specific frequencies, we performed the power spectral density (PSD) analysis. We observed marked differences in the theta with a significantly higher power across many brain areas (FDR corrected Rank-sum test, $P<0.05$) in the AD group in both the left and right hemispheres in Cohort 1 (Fig. 5A and B). Consistently, we observed higher theta power in AD in Cohort 2 (Supplementary Fig. 6A, 6B). In addition, alpha and beta power were reduced in AD in Cohort 2 (Supplementary Fig. 6B). In the prodromal AD group, we observed elevated gamma and delta powers (Fig. 5C and D). Given the differences in signal energy in PSD analysis, we reasoned that ANN would sufficiently classify the groups based on PSD. Indeed, we observed that neural network analysis (see Supplementary Methods) shows 97.73%, and 78.44% classification accuracy in Cohort 1 (AD) and Cohort 3 (prodromal AD), respectively. To understand this further, we performed SHAP, which revealed that theta band contributes predominantly to the classification in AD (Supplementary Fig. 7A); in contrast, the delta and gamma bands contribute in the prodromal AD dataset (Supplementary Fig. 7B). These observations suggest that theta and gamma bands are predominantly altered in AD and prodromal AD, respectively.

Theta is hypoconnected in AD, while gamma is hyperconnected in prodromal AD

We next asked whether EEG functional connectivity also differs in AD and prodromal AD. To test this, we used a pairwise phase consistency (PPC) [46], and performed PPC analysis for all 435 possible combinations from each subject, followed by statistical testing (Rank-sum test with FDR correction for multiple comparisons, $P<0.05$) between control and AD subjects in Cohort 1. Theta connectivity showed significant reductions in AD, and this reduction was widespread across several electrode pairs (Fig. 6A and B, Supplementary Fig. 8A). In addition, alpha and gamma connectivity were reduced primarily between pairs of fronto-parietal and other areas (Fig. 6A and B). The overall PPC was lower in theta, alpha and gamma bands in AD in Cohort 2 (Supplementary Fig. 8B-8D). Next, we compared the PPC between control and prodromal AD subjects in Cohort 3. Interestingly, we observed a significant increase in the connectivity in the gamma in prodromal AD (Fig. 6C and D, Supplementary Fig. 8E). The increase in gamma connectivity in prodromal AD was observed between left fronto-central electrodes and right temporal, parietal, and occipital brain areas (Fig. 6D). Additionally, increased connectivity was observed sporadically in theta and alpha bands in prodromal AD (Fig. 6D). These findings suggest that the signal energy and connectivity of frequency bands affected differ uniquely in AD and prodromal AD.

Discussion

A major contribution of our study is that it provides a comparative analysis examining multiple EEG features spanning various domains with two different preprocessing pipelines, revealing a unique set of EEG features that

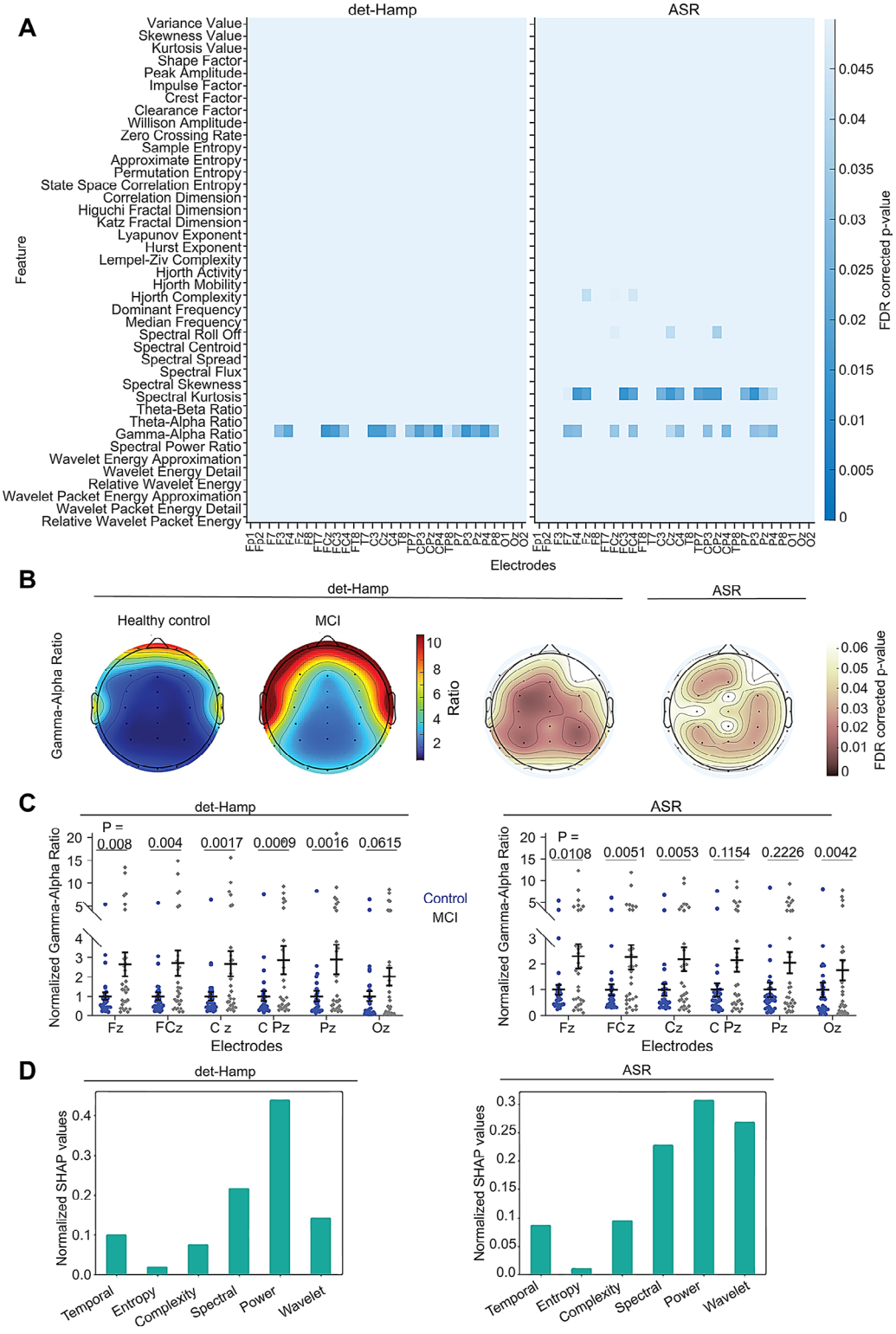

Fig. 4 Enhanced gamma alpha power ratio in prodromal AD. Enhanced gamma/alpha power ratio in prodromal AD. (**A**) Heatmaps show EEG feature differences between healthy control and prodromal AD for the det-Hamp (left) and ASR (right) pipelines after FDR correction. (**B**) The distribution of the gamma/alpha power ratios averaged across all subjects in healthy control (left) and prodromal AD (middle left). The topographic plots with statistically significant scalp locations sustaining FDR correction are shown for the det-Hamp (middle right) and ASR (right) pipelines. (**C**) Plots show the normalized gamma/alpha ratios for det-Hamp (left) and ASR (right, Wilcoxon Rank-sum test) pipelines from Cohort 3 (prodromal AD). Data points represent subjects. (**D**) The normalized cumulative mean of absolute SHAP values are shown

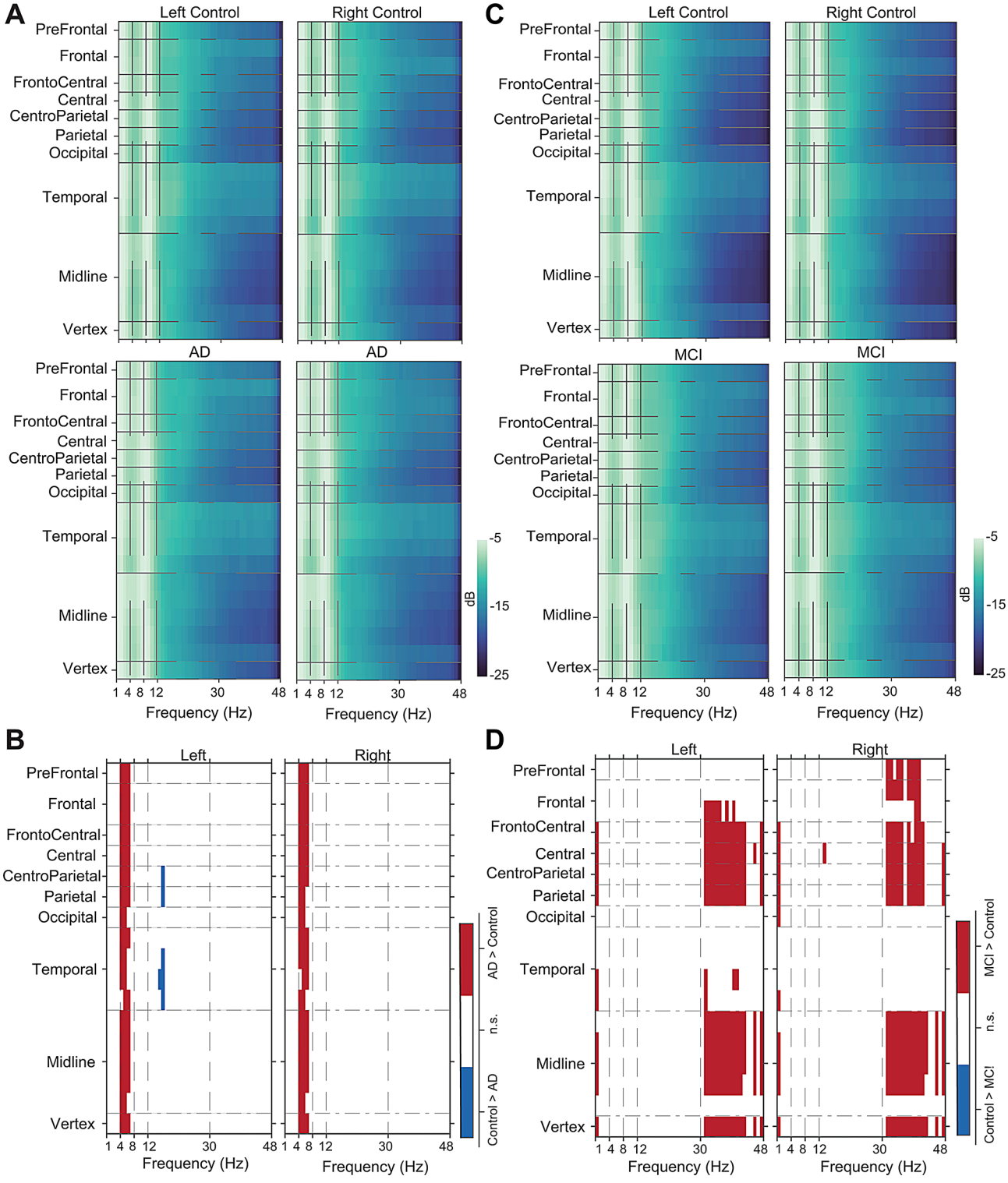

Fig. 5 Changes in theta power in AD and gamma power in prodromal AD. (**A**) Heatmaps show the average EEG power in different areas across left and right brain hemispheres in controls (*N* = 46) and AD subjects (*N* = 46). (**B**) PSD differences between controls and AD after FDR correction. (**C**) Heatmaps show the average EEG power in different areas across left and right brain hemispheres between controls (*N* = 30) and prodromal AD subjects (*N* = 30). (**D**) PSD differences between control and prodromal AD after FDR correction are shown

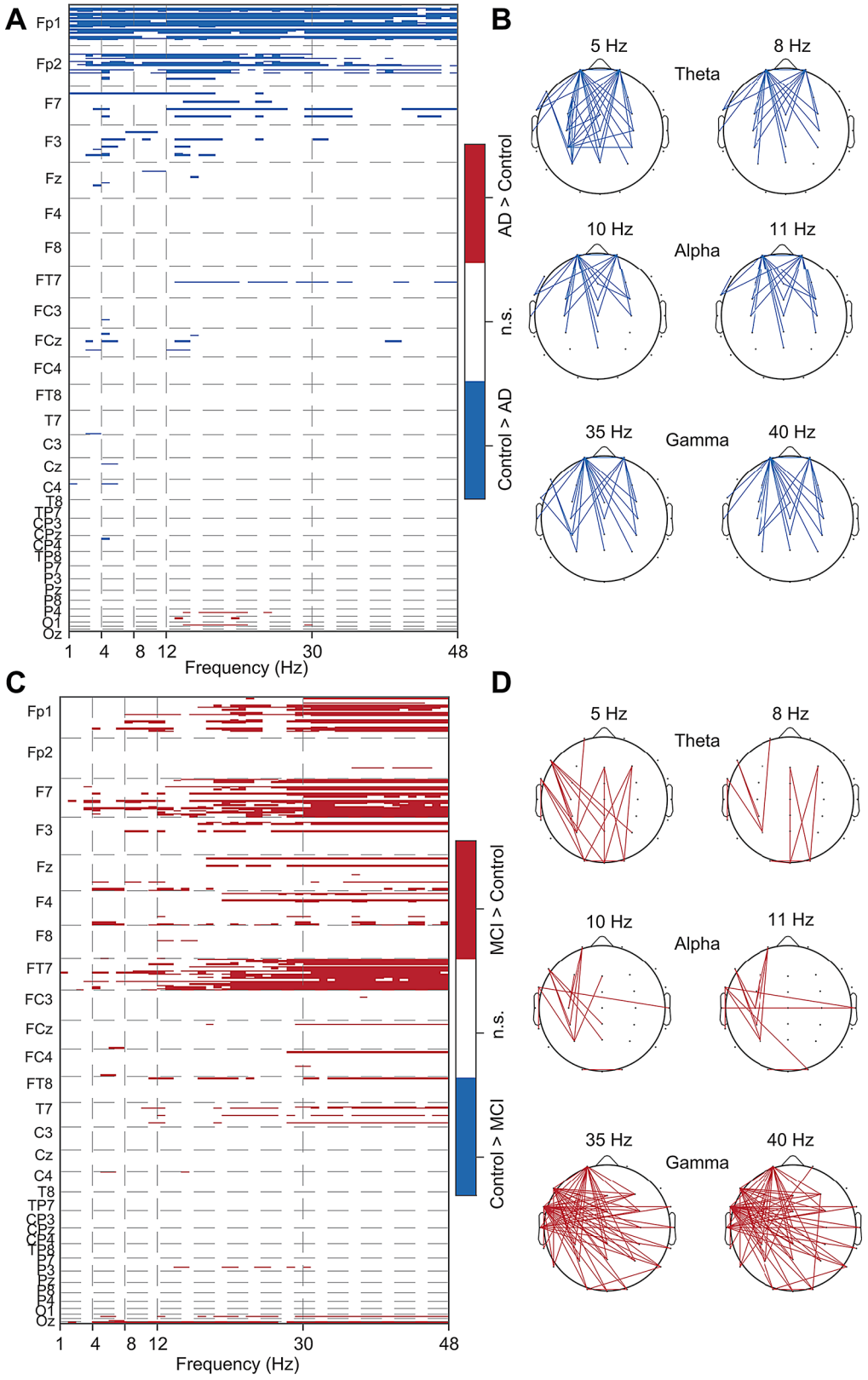

Fig. 6 Altered theta connectivity in AD and gamma connectivity in prodromal AD. (**A**) Heatmap shows the PPC differences between controls and AD. (**B**) The connectivity patterns in AD compared to age-matched control subjects in theta, alpha, and slow gamma bands. (**C**) Heatmap shows the PPC differences between controls and prodromal AD. (**D**) The connectivity patterns in prodromal AD in theta, alpha, and slow gamma bands. The red and blue colors represent the measures studied statistically significantly (FDR corrected $P < 0.05$) higher and lower in AD/prodromal AD than in the control, respectively. The Y- axis labels in the A and C represent the seed electrode for connectivity with other remaining electrodes

significantly deviated in subjects with AD or prodromal AD compared to the age-matched healthy control subjects. Further, we show that brain functional connectivity at the resting state is altered uniquely in AD and prodromal AD.

Changes in the theta/alpha power ratio and theta power in PSD in AD suggest a significant increase in the theta band power. These observations are consistent with a large body of literature [53, 54]. We expanded these observations and examined the topographic distribution of the EEG features and PSD. Our results revealed that theta power was elevated at the whole brain level in AD. The elevated theta power in AD was replicable in two independent cohorts. This suggests the consistency and robustness of the EEG power ratio features, which could be a potential biomarker to differentiate healthy from AD.

Elevated alpha band power in healthy humans during eyes closed state did not differ between healthy and AD subjects in our Cohort 1 after multiple comparison corrections, consistent with previous reports [55]. However, in Cohort 2 and other studies [56] alpha power during the eyes closed state was lower in AD subjects than in healthy subjects. Importantly, we should note that the alpha band was still the dominant oscillatory band in AD in the eyes closed state in both Cohorts 1 and 2 [57]. The eyes-closed state-dependent increase in alpha power is not different between the control and prodromal AD subjects in our study, which is consistent with the previous report [58]. Thus, alpha band power and connectivity are unlikely good markers for AD or prodromal AD [53].

Although alpha oscillations are the most prominent when eyes are closed [59], other bands are also present. The theta power, while not markedly affected in prodromal AD in our study or mildly affected in previous studies [58], was significantly enhanced in AD compared to healthy control subjects and replicated across 2 independent datasets. Recent studies suggest that the periodic components drive the slowing of oscillations in AD [60, 61]. So, what is the underlying mechanism of elevated theta, which is periodic and not coherent between brain areas in AD? The mechanisms of neural oscillations, specifically when eyes are closed, have not been studied at the circuit and cellular level; however, we could speculate that nonessential neuronal ensemble in the local circuit continues to drive theta, in addition to the neuronal ensembles processing alpha in AD. Next, theta is shown to be modulated by acetylcholine [62], and cholinergic defects are observed in AD [63]. Therefore, alterations in cholinergic tone may induce higher theta across many areas in AD, which is another possibility. Finally, a disturbed interaction between ensembles of neurons likely drives different bands of oscillations (theta vs. alpha). Consistently, AD animal model studies demonstrated altered interactions between theta and other bands [64].

Our findings suggest that slowing oscillations (i.e., higher theta power) are specific to AD and not present during the prodromal AD stage. In prodromal AD, the gamma/alpha ratio was higher in several brain areas. Thus, the spectral power change is a non-continuum from prodromal AD, at the group level, to AD. Though the increased delta power was evident in AD and prodromal AD [58], the shift from higher gamma in MCI to higher theta in AD is an interesting observation that requires further studies to examine the underlying circuit and cellular mechanisms.

In addition to the power ratios that robustly distinguish AD and prodromal AD from control subjects, PPC-based brain connectivity also revealed significant differences. We observed that the frequency band and directionality of the changes differed uniquely in AD and prodromal AD. The theta amplitude was higher in AD, but the connectivity was lower brain-wide. Delta and beta bands also showed reduced PPC. In contrast, prodromal AD subjects exhibited higher gamma and stronger connectivity. The differences in the power and connectivity of AD and prodromal AD could not be attributed to age because the age of subjects in AD (70.96 ± 0.81) & MCI (69.4 ± 1.3) in the dataset we used were comparable. A recent study also suggested differences in gamma between AD and MCI [65]. This is consistent with recent observations of hyperconnectivity arising in prodromal AD [66]. Following the administration of FDA-approved acetylcholine esterase inhibitors for one year, gamma power in AD was improved [67]. We speculate that these changes in gamma are likely a compensatory mechanism in prodromal AD [65, 68]. Nonetheless, the gamma offers a marker for prodromal AD.

Although the Lyapunov exponent, Hjorth complexity, and correlation dimensions showed a trend similar to previous findings [14, 69, 70], these measures were not statistically significant after FDR correction for multiple electrode comparisons. Future studies with sufficient sample sizes are required to evaluate their suitability as potential biomarkers.

Our study revealed that EEG features alone are sufficient to distinguish AD or prodromal AD from the age-matched healthy subjects. Preprocessing EEG signals is the most crucial step to understanding the underlying biology [71]. A primary strength of our study was using two independent preprocessing pipelines and observing features that consistently showed similar results in both pipelines. Regardless of the two preprocessing pipelines, most of the results are consistent, suggesting the robustness of the differences we observed in AD and prodromal AD.

Limitations

A limitation of our study is its cross-sectional design- the observations were limited to prodromal AD or AD with their respective age-matched control groups. Therefore, we could not fully understand the trajectory from prodromal AD to AD. Future longitudinal studies are required to fully understand the trajectories of memory impairments. Next, the study included only MMSE scores besides disease diagnosis. Examining the relationship between EEG features, brain imaging and body fluid-based biomarkers, including Aβ, phosphorylated tau, NFL, etc. would provide additional insights [72]. We did not offer interpretations of EEG features that show differences in selective electrodes, pipelines, or datasets, as the differences are inconsistent or not robust.

Conclusion

In conclusion, our study highlights the potential of EEG features as robust biomarkers for distinguishing Alzheimer's disease (AD) and prodromal AD from healthy aging. By employing a comparative analysis across different preprocessing pipelines, we identified unique deviations in EEG patterns, notably elevated theta power in AD, that were consistent across two independent cohorts. The findings reveal the distinct neurophysiological changes between prodromal AD and AD, particularly in oscillatory dynamics and brain connectivity, with theta and gamma power emerging as key differentiators. These insights offer valuable directions for future research into the underlying mechanisms and may pave the way for EEG-based diagnostic tools for early detection and monitoring of Alzheimer's disease.

Supplementary Information

The online version contains supplementary material available at https://doi.org/10.1186/s13195-024-01582-w.

Supplementary Material 1

Supplementary Material 2

Supplementary Material 3

Acknowledgements

We thank Dr. Venkatasubramanian Ganesan and all members of the Chinna lab for their helpful discussions and feedback on the manuscript. We thank CSIR for research fellowships to CAC (CSIR UGC NET, 09/1233(16115)/2022-EMR-I) and HB (CSIR UGC NET, 09/1233(15927)/2022-EMR-I). We also thank the Brain and Behavior Research Foundation for NARSAD young investigator support to CA (#31590), and India Alliance DBT Wellcome Trust Early Career Fellowship to JJ (A/E/22/1/506784).

Author contributions

CA, BG, GY, and JJ conceptualized the project. CA drafted the manuscript. BG, GY, IK, TA, CAC, JJ, PKG, DT, and ASCS developed the methodology. CAC, HB, PKG, and DT analyzed the data. BK, GY, CAC, HB, JJ, DT, and PKG reviewed and edited the manuscript. BK, GY, and CA supervised the project. All authors discussed the results, contributed to the final version, and approved the final manuscript.

Funding

This work was supported by the CBR start-up fund (CA) and the India Alliance DBT Wellcome Trust grant (IA/I/22/1/506257; CA).

Data availability

Datasets 1 and 3 are available from the corresponding author upon reasonable request, and dataset 2 is publicly available online at https://doi.org/10.18112/openneuro.ds004504.v1.0.7. MATLAB codes for extracting 41 EEG features are provided (https://github.com/ChinnakkaruppanAdaikkan/EEG-Features/tree/main), and a stand-alone software tool for EEG feature analysis (Feature Analyzer Installer.exe; Supplementary Material 3).

Declarations

Ethics approval and consent to participate

The study predominantly used previously published datasets. Nonetheless, as described previously [17, 24], all Cohort 1 and 3 participants consented per institutional review board (Istanbul Medipol University, Dokuz Eylül University, or Izmir University of Economics) guidance and regulations. The Cohort 2 dataset has been publicly available.

Consent for publication

Not applicable.

Competing interests

The authors declare no competing interests.

Author details

[1]Centre for Brain Research, Indian Institute of Science, CV Raman Avenue, Bangalore 560 012, India
[2]Neuroscience Research Center, Research Institute for Health Sciences and Technologies (SABITA), Istanbul Medipol University, Istanbul 34810, Turkey
[3]Department of Neuroscience, Health Sciences Institute, Dokuz Eylül University, Izmir 35330, Turkey
[4]Faculty of Medicine, Izmir University of Economics, Izmir 35330, Turkey
[5]Brain Dynamics Research Center, Dokuz Eylül University, Izmir 35330, Turkey
[6]Biomedicine and Genome Center, Izmir 35340, Turkey
[7]Department of Biophysics, School of Medicine, Istanbul Medipol University, Istanbul 34810, Turkey
[8]Manipal Academy of Higher Education, Manipal 576104, India

Received: 30 April 2024 / Accepted: 27 September 2024
Published online: 24 October 2024

References

1. (2023). 2023 Alzheimer's disease facts and figures. Alzheimer's Dement. https://doi.org/10.1002/alz.13016
2. Rowley PA, et al. Amyloid and tau PET imaging of Alzheimer Disease and other neurodegenerative conditions. Seminars Ultrasound CT MRI. 2020. https://doi.org/10.1053/j.sult.2020.08.011.
3. Frontzkowski L, et al. Earlier Alzheimer's disease onset is associated with tau pathology in brain hub regions and facilitated tau spreading. Nat Commun. 2022. https://doi.org/10.1038/s41467-022-32592-7.
4. Liddelow SA, et al. Neurotoxic reactive astrocytes are induced by activated microglia. Nature. 2017. https://doi.org/10.1038/nature21029.
5. van de Haar HJ et al. (2016). Blood-Brain Barrier Leakage in Patients with Early Alzheimer Disease. *Radiology*. https://doi.org/10.1148/radiol.2016152244
6. Bastin C, et al. In vivo imaging of synaptic loss in Alzheimer's disease with [18F]UCB-H positron emission tomography. Eur J Nucl Med Mol Imaging. 2020. https://doi.org/10.1007/s00259-019-04461-x.
7. Wharton W, et al. Neurofibrillary tangles and Conversion to mild cognitive impairment with certain antihypertensives. J Alzheimer's Disease. 2019. https://doi.org/10.3233/JAD-190011.
8. Hatashita S, Wakebe D. Amyloid-β deposition and long-term progression in mild cognitive impairment due to Alzheimer's Disease defined with amyloid PET imaging. J Alzheimer's Disease. 2017. https://doi.org/10.3233/JAD-161074.

9. Cho H, et al. Tau PET in Alzheimer disease and mild cognitive impairment. Neurology. 2016. https://doi.org/10.1212/WNL.0000000000002892.
10. Bejanin A, et al. Tau pathology and neurodegeneration contribute to cognitive impairment in Alzheimer's disease. Brain. 2017. https://doi.org/10.1093/brain/awx243.
11. Gonzalez-Ortiz F, et al. Brain-derived tau: a novel blood-based biomarker for Alzheimer's disease-type neurodegeneration. Brain. 2023. https://doi.org/10.1093/brain/awac407.
12. Hwang G, et al. EEG correlates of verbal and nonverbal working memory. Behav Brain Funct. 2005. https://doi.org/10.1186/1744-9081-1-20.
13. Pedroni A, et al. Automagic: standardized preprocessing of big EEG data. NeuroImage. 2019. https://doi.org/10.1016/j.neuroimage.2019.06.046.
14. Tait L, et al. EEG microstate complexity for aiding early diagnosis of Alzheimer's disease. Sci Rep. 2020. https://doi.org/10.1038/s41598-020-74790-7.
15. Ma MK-H, et al. Regularity and randomness in ageing: differences in resting-state EEG complexity measured by largest Lyapunov exponent. Neuroimage: Rep. 2021. https://doi.org/10.1016/j.ynirp.2021.100054.
16. Safi MS, Safi SMM. Early detection of Alzheimer's disease from EEG signals using Hjorth parameters. Biomed Signal Process Control. 2021. https://doi.org/10.1016/j.bspc.2020.102338.
17. Şeker M, et al. Complexity of EEG Dynamics for early diagnosis of Alzheimer's Disease using permutation Entropy Neuromarker. Comput Methods Programs Biomed. 2021. https://doi.org/10.1016/j.cmpb.2021.106116.
18. Maturana-Candelas A, et al. EEG characterization of the Alzheimer's Disease Continuum by means of Multiscale Entropies. Entropy. 2019. https://doi.org/10.3390/e21060544.
19. Shim Y, et al. Electroencephalography for early detection of Alzheimer's Disease in Subjective Cognitive decline. Dement Neurocognitive Disorders. 2022. https://doi.org/10.12779/dnd.2022.21.4.126.
20. Flores-Sandoval AA, et al. Spectral power ratio as a measure of EEG changes in mild cognitive impairment due to Alzheimer's disease: a case-control study. Neurobiol Aging. 2023. https://doi.org/10.1016/j.neurobiolaging.2023.05.010.
21. Locatelli T, et al. EEG coherence in Alzheimer's disease. Electroencephalogr Clin Neurophysiol. 1998. https://doi.org/10.1016/S0013-4694(97)00129-6.
22. Aoki Y, et al. EEG resting-state networks in Alzheimer's disease associated with clinical symptoms. Sci Rep. 2023. https://doi.org/10.1038/s41598-023-30075-3.
23. Sabbagh MN, et al. FDA position statement early Alzheimer's disease: developing drugs for treatment, Guidance for Industry. Alzheimer's Dementia: Translational Res Clin Interventions. 2019. https://doi.org/10.1016/j.trci.2018.11.004.
24. Güntekin B, et al. Alterations of resting-state Gamma frequency characteristics in aging and Alzheimer's disease. Cogn Neurodyn. 2023. https://doi.org/10.1007/s11571-022-09873-4.
25. Miltiadous A and Katerina D. Tzimourta and Theodora Afrantou and Panagiotis Ioannidis and Nikolaos Grigoriadis and, Dimitrios G, Tsalikakis, Angelidis P, Tsipouras MG. E.G. and N.G. and A.T.T.\; (2024). A dataset of EEG recordings from: Alzheimer's disease, Frontotemporal dementia and Healthy subjects.
26. Robbins KA, et al. How sensitive are EEG results to preprocessing methods: a Benchmarking Study. IEEE Trans Neural Syst Rehabil Eng. 2020. https://doi.org/10.1109/TNSRE.2020.2980223.
27. Coelli S, et al. Selecting methods for a modular EEG pre-processing pipeline: an objective comparison. Biomed Signal Process Control. 2024. https://doi.org/10.1016/j.bspc.2023.105830.
28. Islam MK, et al. Methods for artifact detection and removal from scalp EEG: a review. Neurophysiologie Clinique/Clinical Neurophysiol. 2016. https://doi.org/10.1016/j.neucli.2016.07.002.
29. Chang C-Y, et al. Evaluation of Artifact Subspace Reconstruction for Automatic Artifact Components removal in Multi-channel EEG recordings. IEEE Trans Biomed Eng. 2020. https://doi.org/10.1109/TBME.2019.2930186.
30. de Cheveigné A, Arzounian D. Robust detrending, rereferencing, outlier detection, and inpainting for multichannel data. NeuroImage. 2018. https://doi.org/10.1016/j.neuroimage.2018.01.035.
31. Fujiwara K, et al. Sleep-EEG-based parameters for discriminating fatigue and sleepiness. Front Sleep. 2022. https://doi.org/10.3389/frsle.2022.975415.
32. Delorme A, Makeig S. EEGLAB: an open source toolbox for analysis of single-trial EEG dynamics including independent component analysis. J Neurosci Methods. 2004. https://doi.org/10.1016/j.jneumeth.2003.10.009.
33. Dagar M et al. (2018). Performance Comparison of Hampel and Median Filters in Removing Deep Brain Stimulation Artifact, pp. 17–28.
34. Bokil H, et al. Chronux: a platform for analyzing neural signals. J Neurosci Methods. 2010. https://doi.org/10.1016/j.jneumeth.2010.06.020.
35. Kothe. (2015). Artifact removal technique with signal reconstruction. issued 2015.
36. Willison. (1963). *J.Physiology*.
37. Giannakopoulos T, Pikrakis A. Audio features. Introduction to Audio Analysis. Elsevier; 2014. pp. 59–103. https://doi.org/10.1016/C2012-0-03524-7.
38. Tripathy RK, et al. Analysis of physiological signals using state space correlation entropy. Healthc Technol Lett. 2017. https://doi.org/10.1049/htl.2016.0065.
39. Richman JS, Moorman JR. Physiological time-series analysis using approximate entropy and sample entropy. Am J Physiol Heart Circ Physiol. 2000. https://doi.org/10.1152/ajpheart.2000.278.6.H2039.
40. Germán-Salló Z. Measuring the complexity of Discrete signals. Procedia Manuf. 2020. https://doi.org/10.1016/j.promfg.2020.03.080.
41. Choi J, et al. Resting-state prefrontal EEG biomarkers in correlation with MMSE scores in elderly individuals. Sci Rep. 2019. https://doi.org/10.1038/s41598-019-46789-2.
42. Baik K, et al. Implication of EEG theta/alpha and theta/beta ratio in Alzheimer's and Lewy body disease. Sci Rep. 2022. https://doi.org/10.1038/s41598-022-21951-5.
43. Özbek Y, et al. Resting-state EEG alpha/theta power ratio discriminates early-onset Alzheimer's disease from healthy controls. Clin Neurophysiol. 2021. https://doi.org/10.1016/j.clinph.2021.05.012.
44. AlSharabi K, et al. EEG Signal Processing for Alzheimer's disorders using Discrete Wavelet Transform and Machine Learning approaches. IEEE Access. 2022. https://doi.org/10.1109/ACCESS.2022.3198988.
45. Oostenveld R, et al. FieldTrip: Open Source Software for Advanced Analysis of MEG, EEG, and Invasive Electrophysiological Data. Comput Intell Neurosci. 2011. https://doi.org/10.1155/2011/156869.
46. Vinck M, et al. The pairwise phase consistency: a bias-free measure of rhythmic neuronal synchronization. NeuroImage. 2010. https://doi.org/10.1016/j.neuroimage.2010.01.073.
47. Hollander M, et al. Nonparametric statistical methods. Wiley; 2015.
48. (2011). Nonparametric Statistical Inference by GIBBONS, J. D. and CHAKRABORTI S. *Biometrics*. https://doi.org/10.1111/j.1541-0420.2011.01658_9.x
49. Benjamini Y, Hochberg Y. Controlling the false Discovery rate: a practical and powerful Approach to multiple testing. J Roy Stat Soc: Ser B (Methodol). 1995. https://doi.org/10.1111/j.2517-6161.1995.tb02031.x.
50. Sedgwick P. Spearman's rank correlation coefficient. BMJ. 2014. https://doi.org/10.1136/bmj.g7327.
51. Benz N, et al. Slowing of EEG background activity in Parkinson's and Alzheimer's disease with early cognitive dysfunction. Front Aging Neurosci. 2014. https://doi.org/10.3389/fnagi.2014.00314.
52. Wiesman AI, et al. Spatially resolved neural slowing predicts impairment and amyloid burden in Alzheimer's disease. Brain. 2022. https://doi.org/10.1093/brain/awab430.
53. Moretti D. Individual analysis of EEG frequency and band power in mild Alzheimer's disease. Clin Neurophysiol. 2004. https://doi.org/10.1016/S1388-2457(03)00345-6.
54. Coben LA, et al. Frequency analysis of the resting awake EEG in mild senile dementia of Alzheimer type. Electroencephalogr Clin Neurophysiol. 1983. https://doi.org/10.1016/0013-4694(83)90124-4.
55. Murty DV, et al. Stimulus-induced gamma rhythms are weaker in human elderly with mild cognitive impairment and Alzheimer's disease. eLife. 2021. https://doi.org/10.7554/eLife.61666.
56. Zhang H, et al. The significance of EEG Alpha Oscillation Spectral Power and Beta Oscillation Phase synchronization for diagnosing probable Alzheimer Disease. Front Aging Neurosci. 2021. https://doi.org/10.3389/fnagi.2021.631587.
57. Gaubert S, et al. EEG evidence of compensatory mechanisms in preclinical Alzheimer's disease. Brain. 2019. https://doi.org/10.1093/brain/awz150.
58. Meghdadi AH, et al. Resting state EEG biomarkers of cognitive decline associated with Alzheimer's disease and mild cognitive impairment. PLoS ONE. 2021. https://doi.org/10.1371/journal.pone.0244180.
59. Hohaia W, et al. Occipital alpha-band brain waves when the eyes are closed are shaped by ongoing visual processes. Sci Rep. 2022. https://doi.org/10.1038/s41598-022-05289-6.
60. Kopčanová M, et al. Resting-state EEG signatures of Alzheimer's disease are driven by periodic but not aperiodic changes. Neurobiol Dis. 2024. https://doi.org/10.1016/j.nbd.2023.106380.

61. Azami H, et al. Beta to theta power ratio in EEG periodic components as a potential biomarker in mild cognitive impairment and Alzheimer's dementia. Alzheimer's Res Therapy. 2023. https://doi.org/10.1186/s13195-023-01280-z.
62. Gedankien T, et al. Acetylcholine modulates the temporal dynamics of human theta oscillations during memory. Nat Commun. 2023. https://doi.org/10.1038/s41467-023-41025-y.
63. Whitehouse PJ, et al. Alzheimer disease: evidence for selective loss of cholinergic neurons in the nucleus basalis. Ann Neurol. 1981. https://doi.org/10.1002/ana.410100203.
64. Wirt RA, et al. Altered theta rhythm and hippocampal-cortical interactions underlie working memory deficits in a hyperglycemia risk factor model of Alzheimer's disease. Commun Biology. 2021. https://doi.org/10.1038/s42003-021-02558-4.
65. van Deursen JA, et al. Increased EEG gamma band activity in Alzheimer's disease and mild cognitive impairment. J Neural Transm. 2008. https://doi.org/10.1007/s00702-008-0083-y.
66. Fide E, et al. Hyperconnectivity matters in early-onset Alzheimer's disease: a resting-state EEG connectivity study. Neurophysiol Clin. 2022. https://doi.org/10.1016/j.neucli.2022.10.003.
67. Fide E, et al. Normalized Theta but increased Gamma activity after acetylcholinesterase inhibitor treatment in Alzheimer's Disease: preliminary qEEG Study. Clin EEG Neurosci. 2023. https://doi.org/10.1177/15500594221120723.
68. Aurtenetxe S, et al. Dysfunctional and compensatory duality in mild cognitive impairment during a continuous recognition memory task. Int J Psychophysiol. 2013. https://doi.org/10.1016/j.ijpsycho.2012.11.008.
69. Jiao B, et al. Neural biomarker diagnosis and prediction to mild cognitive impairment and Alzheimer's disease using EEG technology. Alzheimer's Res Therapy. 2023. https://doi.org/10.1186/s13195-023-01181-1.
70. Tzimourta KD, et al. Analysis of electroencephalographic signals complexity regarding Alzheimer's Disease. Comput Electr Eng. 2019. https://doi.org/10.1016/j.compeleceng.2019.03.018.
71. Kim S-P. (2018). Preprocessing of EEG, pp. 15–33.
72. Moretti, D. (2015). Association of EEG, MRI, and regional blood flow biomarkers is predictive of prodromal Alzheimer’s disease. *Neuropsychiatric Disease and Treatment*. https://doi.org/10.2147/NDT.S93253.

Publisher's note